OPEN

Citation: Cell Death and Disease (2014) 5, e1223; doi:10.1038/cddis.2014.188

www.nature.com/cddis

Combined PDK1 and CHK1 inhibition is required to kill glioblastoma stem-like cells *in vitro* and *in vivo*

M Signore*[,1], F Pelacchi[1], S di Martino[2], D Runci[1], M Biffoni[1], S Giannetti[3], L Morgante[3], M De Majo[1], EF Petricoin[4], L Stancato[5], LM Larocca[6], R De Maria[2], R Pallini[7,8] and L Ricci-Vitiani*[,1,8]

Glioblastoma (GBM) is the most common and deadly adult brain tumor. Despite aggressive surgery, radiation, and chemotherapy, the life expectancy of patients diagnosed with GBM is ~14 months. The extremely aggressive nature of GBM results from glioblastoma stem-like cells (GSCs) that sustain GBM growth, survive intensive chemotherapy, and give rise to tumor recurrence. There is accumulating evidence revealing that GSC resilience is because of concomitant activation of multiple survival pathways. In order to decode the signal transduction networks responsible for the malignant properties of GSCs, we analyzed a collection of GSC lines using a dual, but complementary, experimental approach, that is, reverse-phase protein microarrays (RPPMs) and kinase inhibitor library screening. We treated GSCs *in vitro* with clinically relevant concentrations of temozolomide (TMZ) and performed RPPM to detect changes in phosphorylation patterns that could be associated with resistance. In addition, we screened GSCs *in vitro* with a library of protein and lipid kinase inhibitors to identify specific targets involved in GSC survival and proliferation. We show that GSCs are relatively insensitive to TMZ treatment in terms of pathway activation and, although displaying heterogeneous individual phospho-proteomic profiles, most GSCs are resistant to specific inhibition of the major signaling pathways involved in cell survival and proliferation. However, simultaneous multipathway inhibition by the staurosporin derivative UCN-01 results in remarkable inhibition of GSC growth *in vitro*. The activity of UCN-01 on GSCs was confirmed in two *in vivo* models of GBM growth. Finally, we used RPPM to study the molecular and functional effects of UCN-01 and demonstrated that the sensitivity to UCN-01 correlates with activation of survival signals mediated by PDK1 and the DNA damage response initiated by CHK1. Taken together, our results suggest that a combined inhibition of PDK1 and CHK1 represents a potentially effective therapeutic approach to reduce the growth of human GBM.
Cell Death and Disease (2014) **5,** e1223; doi:10.1038/cddis.2014.188; published online 8 May 2014
Subject Category: Cancer

Glioblastoma multiforme (GBM) is the second most common brain tumor in people aged from 55 to 84 years.[1] Current standard therapy, including maximal safe resection followed by radiotherapy in combination with temozolomide (TMZ), does not yield definitive effects and a majority of patients succumb to the disease within 2 years after diagnosis.[2] One of the major hurdles to surgical resection and the major cause of relapse is the invasive nature of GBM and its intrinsic resistance to therapy.[3,4] Such tumorigenic properties have been ascribed to a rare fraction of self-renewing, multipotent tumor-initiating cells, GBM stem-like cells (GSCs), responsible for tumor progression, maintenance, and recurrence.[5–7] GSCs play a critical role in both invasiveness and chemo- and radio-resistance of GBM.[8,9] Moreover, GSCs may sustain tumor angiogenesis by vascular differentiation.[10,11] These characteristics make their elimination an extremely difficult task.

The recent characterization of the human cancer genome (Cancer Genome Atlas Research Network, 2008; http://cancergenome.nih.gov/)[12] and transcriptome[13,14] of GBM has provided a high-resolution picture that has revealed the major gene alterations that may drive disease pathogenesis and biology. The commonly altered genes include *EGF-R* (~40%), *PTEN* (37%), *PIK3CA* (13%), *PIK3R1* (8%), and *PDGFRA* (8%). Over 80% of GBMs have an acquired alteration in the RTK/PI3K/AKT pathway with ~40% of tumors having some alteration in EGF-R. These comprehensive data sets reveal GBM as a heterogeneous collection of distinct diseases with multiple dependencies both within and across each particular subtype. Despite apparent single pathway perturbations found in GBM, specific target drugs, including those that target AKT/mTOR, did not show clinical efficacy.[15] DNA alterations may not translate to protein derangements and often times the DNA–protein correlations are weak. Therefore, to further dissect GBM signaling pathways and to find appropriate clinical targets to be exploited for drug discovery, several investigators have attempted to

[1]Department of Hematology, Oncology and Molecular Medicine, Istituto Superiore di Sanità, Rome, Italy; [2]Italian National Cancer Institute 'Regina Elena', Rome, Italy; [3]Institute of Human Anatomy, Università Cattolica del Sacro Cuore, Rome, Italy; [4]Center for Applied Proteomics and Molecular Medicine, George Mason University, Manassas, VA, USA; [5]Cancer Biology and Patient Tailoring, Discovery Oncology, Eli Lilly and Company, Indianapolis, IN, USA; [6]Institute of Pathology, Università Cattolica del Sacro Cuore, Rome, Italy and [7]Institute of Neurosurgery, Università Cattolica del Sacro Cuore, Rome, Italy
*Corresponding authors: M Signore or L Ricci-Vitiani, Department of Hematology, Oncology and Molecular Medicine, Istituto Superiore di Sanità, Viale Regina Elena 299, Rome 00161, Italy. Tel: +39 6 49904453 (MS) or +39 6 49903673 (LR-V); Fax: +39 6 49387087; E-mail: michele.signore@iss.it or lriccivitiani@yahoo.it
[8]These authors shared senior authorship.
Keywords: glioblastoma stem-like cells; phospho-proteomics; kinase inhibitors; PDK1; DNA damage
Abbreviations: GBM, glioblastoma multiforme; TMZ, temozolomide; GSC, glioblastoma stem-like cell; RPPM, reverse-phase protein microarray
Received 25.10.13; revised 28.3.14; accepted 31.3.14; Edited by RA Knight

characterize GSCs at the molecular and functional levels. EGF-R signaling is known to substantially contribute to GBM malignancy and, using a mass spectrometry-based approach, Kozuka-Hata *et al.*[16] performed a comprehensive analysis of the phospho-proteome of GSCs in response to EGF stimulation. They identified multiple signaling pathway perturbations with calcium-dependent protein kinase C (PKC), AKT, and CHK1/2 significantly modulated by EGF. Growing evidence reveals that GSCs display extensive multiple kinase activation,[17] and therefore sustained activation of multiple non-overlapping signaling pathways could be a major issue in therapeutic intervention.[18–20] Recent advances in the development of small molecules and the broad spectrum of activity exhibited by several FDA-approved drugs[21] may help to identify novel small molecule therapies for GBM.

Commercially available immortalized cancer cell lines cannot account for the genetic diversity between patients or for the heterogeneity of tumor cells. Novel approaches directed at eradicating GBM could be greatly strengthened by the use of patient-derived GSCs that more closely mimic primary GBM. In the present work, we analyzed a diverse collection of GSC lines[22] by combining a powerful phospho-proteomic platform (reverse-phase protein microarrays, RPPMs), with small molecule kinase inhibitor library screening, aimed at identifying and interrogating signaling pathways involved in GSC resistance to therapy.

Results

GSCs are resistant to TMZ and their pathway activation pattern is not influenced by treatment. TMZ is the current standard of care for patients with GBM; however, only a minority of patients survives for >3 years. We successfully isolated and characterized stem-like cell lines from several GBM patients. These cells exhibit tumorigenic properties *in vitro* and *in vivo* and represent a powerful tool for molecular investigation of GBM.[3,22,23] Most of the GSCs used in the present study are resistant *in vitro* to clinically relevant concentrations of TMZ,[24] irrespective of their *MGMT* or *PTEN* status (Figure 1a and Supplementary Table S1), as previously reported.[3] Among the available technologies in proteomics, RPPM represents one of the most flexible and robust technology,[25,26] providing quantitative broad-scale measurement of hundreds of phosphoproteins, even low abundance signaling molecules that are below the detection limits of mass spectrometry. To understand whether TMZ resistance correlated with specific signal transduction pathway activation, we performed RPPM analysis on lysates from GSCs treated for 72 h with TMZ. Incubation time was selected after preliminary time course evaluation (Supplementary Figure S1). Hierarchical clustering of proteins involved in survival and proliferation showed that pathway activation mainly groups by GSC line rather than by treatment (Figure 1b). GSCs do not show major changes in their pathway activation profile and most GSCs display differential activation of nodes in the same pathways, pointing to a molecular differentiation based on rearrangement of the signaling network rather than differential activation of parallel pathways (Supplementary Table S2).

Small molecule kinase inhibitor library screening identifies potential therapeutic targets. Our phospho-proteomic-based pathway activation mapping analysis suggested that the intrinsic resistance of GSCs to cytotoxic drugs is dependent upon constitutively active pro-survival pathways and confirms previous findings reported by other investigators.[17–20] Therefore, we decided to treat GSCs with a commercially available small molecule kinase inhibitor library composed of 80 different compounds targeting a multitude of human protein or lipid kinases (Supplementary Table S3). The two GSC lines assayed displayed marked resistance to most of the compounds tested, whereas inhibition of PKC (rottlerin and Ro 31–8220) or ERK2/adenosine kinase (5-iodotubercidin), PDGF-R (tyrphostin 9), and EGF-R (erbstatin analog) inhibitors yielded significant antiproliferative results (Figure 2a). Our functional data derived from *in vitro* kinase inhibition confirm the existence of strong survival signals in GSCs that confer resistance to targeted inhibition.

As the specificity of kinase inhibitors can vary with compound concentration (i.e., increasing concentration often yields increasing off-target effects), we performed titration assays to better understand the specificity of the compounds found effective in the library screening at relatively high concentration (Figure 2b). Most of the compounds were inactive at submicromolar concentrations, as shown by markedly high EC_{50} values for all cell lines. Thus, we tested compounds with analog target specificity in order to verify previous results (Figures 2b–d). These analog compounds included a preclinical ERK inhibitor and two compounds already in use in the clinics (gefitinib and sorafenib, Figure 2c) and, as two out of the five positive hits had PKC as the primary target, we used an additional set of inhibitors against this kinase (Figure 2d). One of the PKC inhibitors, the staurosporine derivative UCN-01 (7-hydroxy-staurosporine), was the most effective antiproliferative agent, yielding a range of sensitivity across the GSC lines. We classified GSCs into three sensitivity groups, that is, low, medium, and high, based on the relative efficacy of UCN-01. The commercial cell line T98G was more sensitive than any GSC, whereas U87MG was included in the low-sensitivity group (Table 1). Normal neural stem cells[27] were less sensitive than GSCs and sensitivity to UCN-01 markedly increased after *in vitro* differentiation (Supplementary Figure S2). To confirm the ability of UCN-01 to induce cell death, we evaluated DNA content in GSCs treated with the compound. The increase in the pre-G_0 peak in the treated samples as compared with control correlated with the sensitivity displayed by GSCs in the ATP-based assay (Supplementary Figures S3a and b). Microscopic examination of GSCs treated with UCN-01 confirmed the presence of morphological (AO/PI) and functional (TUNEL) signatures of apoptosis mainly in the highly sensitive lines (Supplementary Figure S3c).

UCN-01 cytotoxic effect is mediated by PDK1 and CHK1 inhibition. UCN-01 is a potent inhibitor of CHK1 ($K_i = 5.6$ nM), 3′-phosphoinositide-dependent protein kinase-1 (PDK1; $IC_{50} = 5.0$ nM), PKCβ ($IC_{50} = 10$ nM), and CDKs (K_i: CDK1 and CDC2 95 nM, CDK2 30 nM, and CDK4 3.6 μM), and other PKC isoforms ($IC_{50} < 1\ \mu$M) are inhibited with a lower potency.[28–31] Despite the fact that both staurosporine

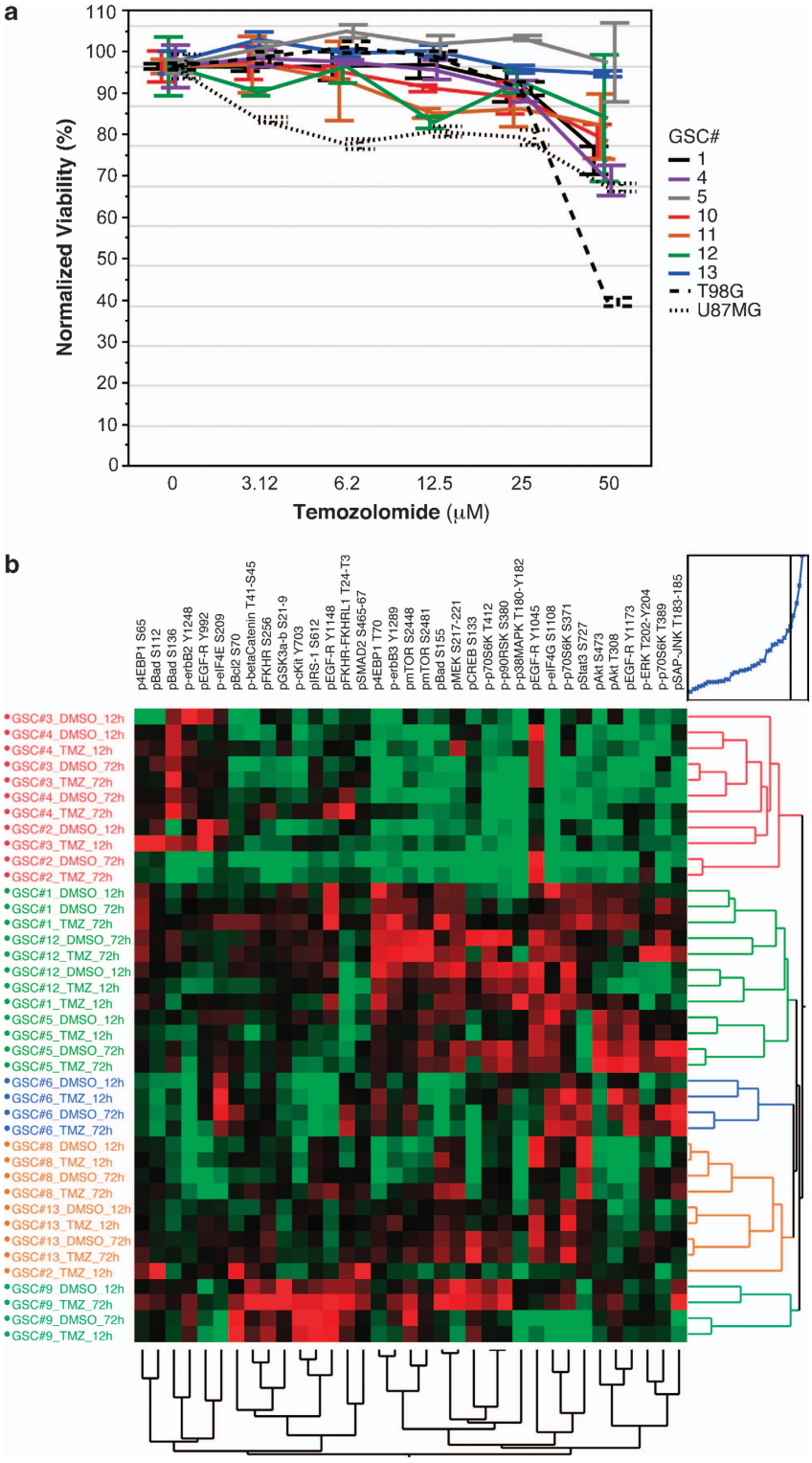

Figure 1 TMZ treatment and RPPM analysis of GSCs. (**a**) A collection of GSCs and two commercially available GBM cell lines have been treated with increasing doses of TMZ and viability was measured at 72 h. Data are represented as mean ± S.E.M. from at least three independent experiments. (**b**) Hierarchical clustering of RPPM data (mean of three technical replicates) obtained by assaying a panel of antibodies mainly directed against components of the EGF-R and PI3-K/AKT/mTOR pathways on protein lysates of selected GSC lines treated either with vehicle (DMSO) or with 50 μM TMZ for either 12 or 72 h. Colored clusters were selected by cutting the dendrogram at the height indicated in the upper-right hierarchy plot. A summary of the phosphoproteins present in each cluster is available as Supplementary Table S2

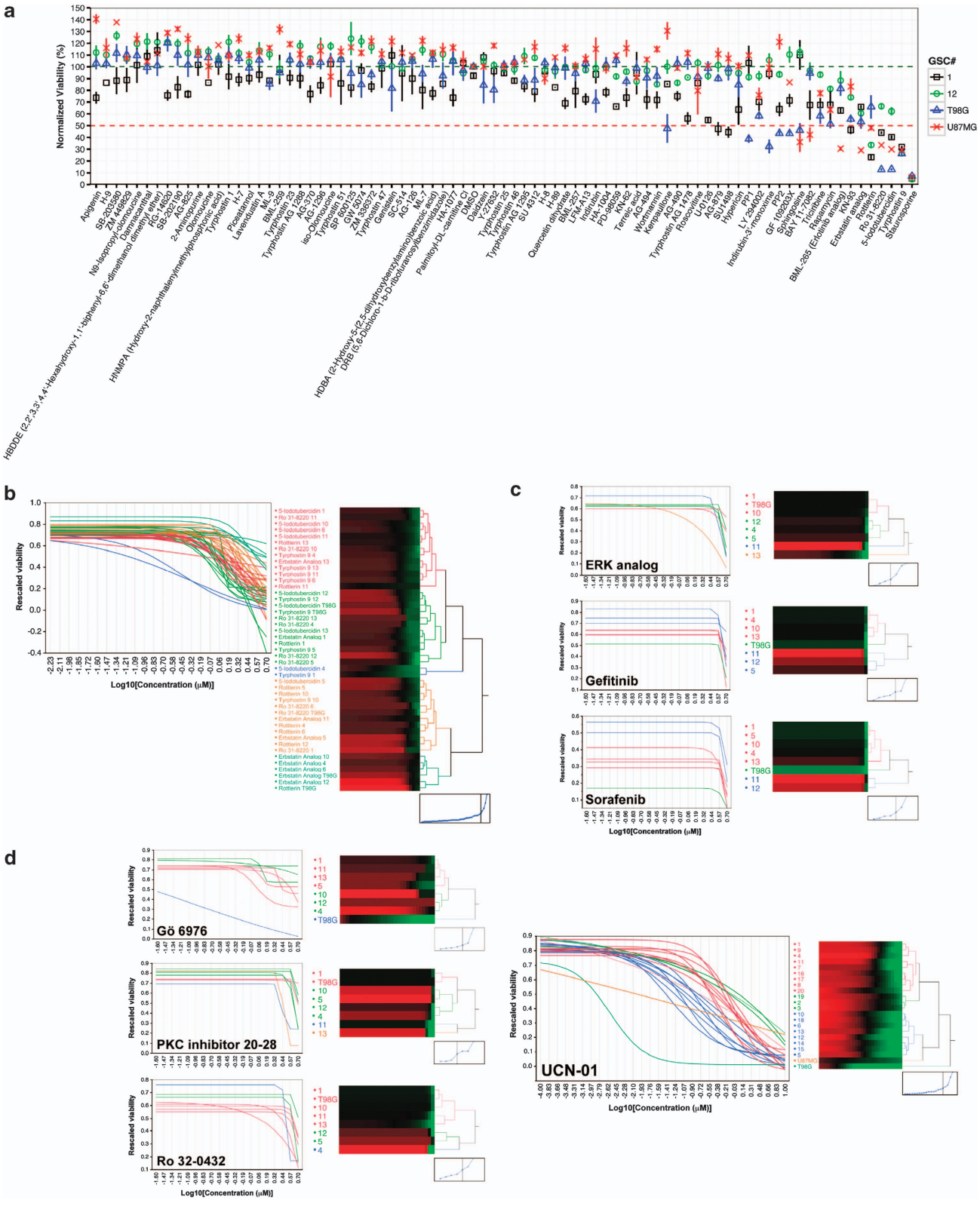

Figure 2 Kinase inhibitor library screening and titration assays of positive hits and analogs in GSCs. (**a**) Point chart of the viability of two GSCs and two commercial GBM cell lines treated with the kinase inhibitor library each compound at 5 μM for 72 h. Normalized viability of each cell line is plotted as mean ± S.D. from three independent experiments. Horizontal dashed lines represent reference lines for 100% (dark green) and 50% (red) viability. (**b**) Parallel plots of fitted 4PL curves and correspondent hierarchical clustering maps of pEC_{50} values (see Materials and Methods section for details) derived from titration curves of GSCs treated for 72 h with positive hits from the library screening and (**c** and **d**) analog compounds. Fitting was performed on individual dose-response curves obtained from three independent experiments

Table 1 EC_{50} calculated after 72 h of treatment with UCN-01

GSC no.	EC_{50} (μM)	Sensitivity
T98G	0.003	High
12	0.043	High
15	0.090	High
5	0.094	High
14	0.184	High
13	0.221	High
10	0.242	High
11	0.367	Medium
18	0.414	Medium
7	0.548	Medium
4	0.581	Medium
6	0.628	Medium
8	0.805	Medium
9	0.949	Medium
1	1.436	Low
17	1.938	Low
U87MG	2.711	Low
16	3.416	Low
3	4269.117	Low
20	79056.358	Low
2	227826.165	Low
19	341092.047	Low

Sensitivity range: high <250 nM; 250 nM $<$ medium $<1\,\mu$M; low $>1\,\mu$M. GSC lines are ordered by their sensitivity to UCN-01

and UCN-01 are relatively nonspecific inhibitors, the activity of UCN-01 is significantly different from that of staurosporine.[29,32] In order to investigate which UCN-01 target(s) was involved in GSC death, we treated three GSCs lines for each UCN-01 sensitivity group, and analyzed the levels of total and phosphorylated PDK1 (S241), PKCα/βII (T638-41), CDC25C (S216), and CDC2 (Y15) (Figures 3a and b and Supplementary Figure S4a). Downmodulation of the autophosphorylation site of PKCα/βII, as well as of total PKCα was present in all GSCs only at the highest concentration tested. Conversely, only GSC 12 among the highly sensitive lines showed an appreciable reduction in PDK1 and its autophosphorylated form, PDK1 S241 (Figures 3a and b). PDK1 was heavily phosphorylated in the low-sensitivity line GSC1 but, although basal levels of PDK1 S241 did not show significant difference among GSCs from different sensitivity groups (Figures 3a and b and Supplementary Figure S5), the ratio between phospho- and total PDK1 was significantly higher in the sensitive GSC lines (Supplementary Figure S4b). As expected, because of their functional proximity to CHK1, one of the main targets of UCN-01, the phosphorylation of CDC25C and its downstream interactor CDC2 also exhibited a concentration-dependent downregulation in all three sensitivity groups (Figures 3a and b and 4).

In order to better understand the molecular mechanisms underlying the differential sensitivity to UCN-01 found in GSCs, we performed an extensive RPPM analysis on the same three GSC lines from each group after 48 and 72 h of treatment. Differently from TMZ, treatment with UCN-01 caused molecular changes in nearly all of the GSC lines (Figure 4a). Interestingly, the effects of UCN-01 were not significantly different between the time points, and although a completely neat distinction of GSCs based on their UCN-01 sensitivity was not present in the RPPM heatmap profiles, most low-sensitivity GSCs formed compact clusters separated from the highly sensitive GSC lines (Figure 4a). The medium-sensitivity group displayed intermediate molecular patterns and, at the highest concentration of UCN-01, GSCs from diverse sensitivity groups clustered much closer. A deeper analysis made on each individual group of sensitivity showed that clearly divergent clusters at concentrations $<1\,\mu$M are present only for the high-sensitivity GSCs (Supplementary Figure S5a). Although a significant difference between low/medium- and high-sensitivity GSCs was not present in terms of caspase activation and initiation of DNA damage response through phosphorylation of histone H2A.Xγ, cells that are highly sensitive to UCN-01 displayed high basal pAKT S473 and pAKT T308 but low BCL2 (Figure 4b and Supplementary Figure S5b). More important, although UCN-01 reduced pBAD S112 in all GSCs in a concentration-dependent manner, the levels of pAKT T308, which is the direct phosphorylation target of PDK1, rapidly and specifically decreased only in highly sensitive GSCs. Conversely, the high levels of pAKT S473, which is the main phosphorylation target of the mTORC2 complex,[33] correlated only in highly sensitive GSCs with most end points involved in the mTOR pathway (Figure 4b). Furthermore, low- and medium-sensitive GSCs displayed lower levels of pRPA2 S4–8, pATR S428, pCHK1 S345, and pCDC25C S216 compared with the high-sensitivity lines. RPPM data confirmed western blot results and, in line with this molecular scenario, low- and medium-sensitive GSCs exhibited high levels of pWEE1 S642 and pATM S1981, although CHK2, which is the main effector of ATM, was more phosphorylated in the low-sensitivity group only. Interestingly, Cyclin B1 and Cyclin D1 were significantly elevated in highly sensitive GSCs (Figure 4b and Supplementary Figure S5b). In order to assess the statistical significance of the aforementioned molecular differences between GSCs that are markedly affected by UCN-01 compared with the others, we performed statistical analyses (Supplementary Table S4) and produced multistate activation maps for cell cycle or PI3K/AKT pathways that provide an overall view of the molecular signatures of GSCs (Supplementary Figure S6). In addition, to evaluate the relative impact of target inhibition by UCN-01, we treated three GSC lines, one selected from each UCN-01 sensitivity group, with small molecule kinase inhibitors directed against PKC, PDK1, or CHK1 and performed an *in vitro* drug combination assay (Supplementary Figure S7). Inhibition of PKC did not cause cytotoxicity, whereas simultaneous inhibition of CHK1 (AZD7762) and PDK1 (OSU-03012) at concentrations twofold lower than individual EC_{50} produced synergistic effects on all GSCs and reproduced the sensitivity pattern observed with UCN-01. Taken together, these data suggest that addiction to DNA damage and PI3K/AKT/mTOR pathways may be associated with sensitivity to UCN-01 in GSCs.

UCN-01 significantly reduces the growth of GSC intracerebral xenografts. Intracerebral injection of GSCs into immunodeficient mice generates highly infiltrative tumor xenografts that closely mimic the behavior of malignant gliomas.[22,23,34,35] Within a few weeks after grafting, the GSCs colonize the injection site and spread toward distant brain regions with a special tropism for the large paths of

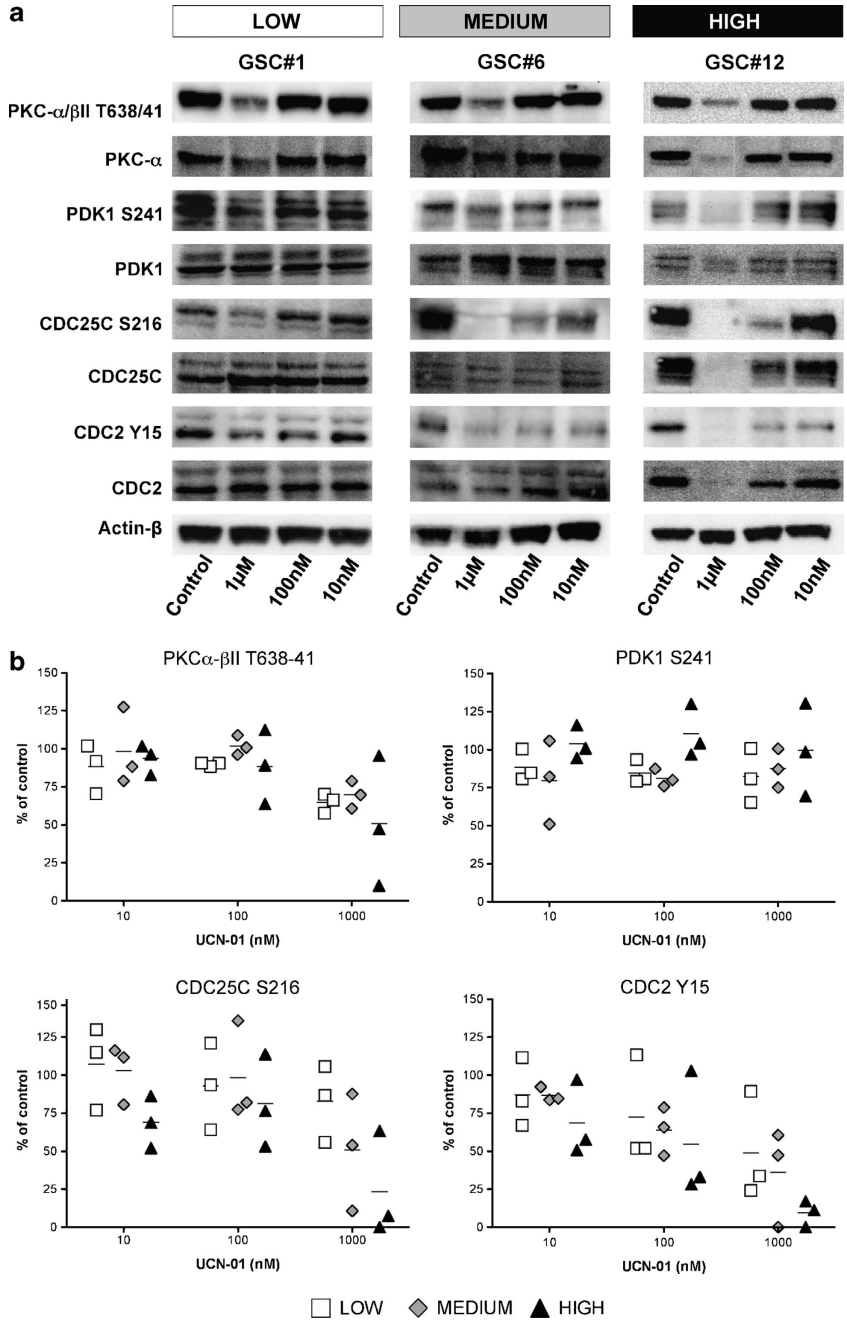

Figure 3 Immunoblot analysis of UCN-01 targets. (**a**) GSC lines selected from each sensitivity group were exposed to increasing doses of UCN-01 and the phosphorylation levels of PKC, PDK1, CDC25C, and CDK1 (CDC2) were evaluated at 72 h. Representative blots are shown for three GSC lines (Supplementary Figure S4 displays the blots performed on the other tested GSC lines in each sensitivity group). (**b**) Normalized intensities of the immunoblot bands from each antibody tested are plotted for all three GSC lines in each sensitivity group as percentage over the untreated control. No statistically significant difference between sensitivity groups at various UCN-01 concentrations was found after two-way ANOVA and Bonferroni post test

white matter. We used brain xenografts of GSCs as an experimental paradigm to assess whether UCN-01 retains its antitumor effect *in vivo*. Stable green fluorescence protein (GFP)-expressing GSC line 1, belonging to the low-sensitivity group that shows the same *in vitro* response to UCN-01 as the parental line (data not shown), was grafted into the striatum of NOD-SCID mice. We coadministered UCN-01 (1 μM) or vehicle (DMSO) directly with the GSC inoculation to overcome possible problems of blood brain barrier (BBB) penetrance. At 8 weeks after grafting, control mice ($n=6$) harbored tumors that invaded the homolateral striatum, piriform cortex, corpus callosum, anterior commissure, internal capsule, optic tract, septal nuclei, and fimbria-hippocampus (Figure 5a), whereas the degree of brain invasion was significantly reduced in UCN-01-treated mice ($n=6$, Figure 5b). The volume of the brain region invaded by GFP^+ GSCs was 10.46 ± 0.83 and $0.78 \pm 0.19\,mm^3$ (mean $\pm$ S.E.M.) in control and UCN-01-treated mice,

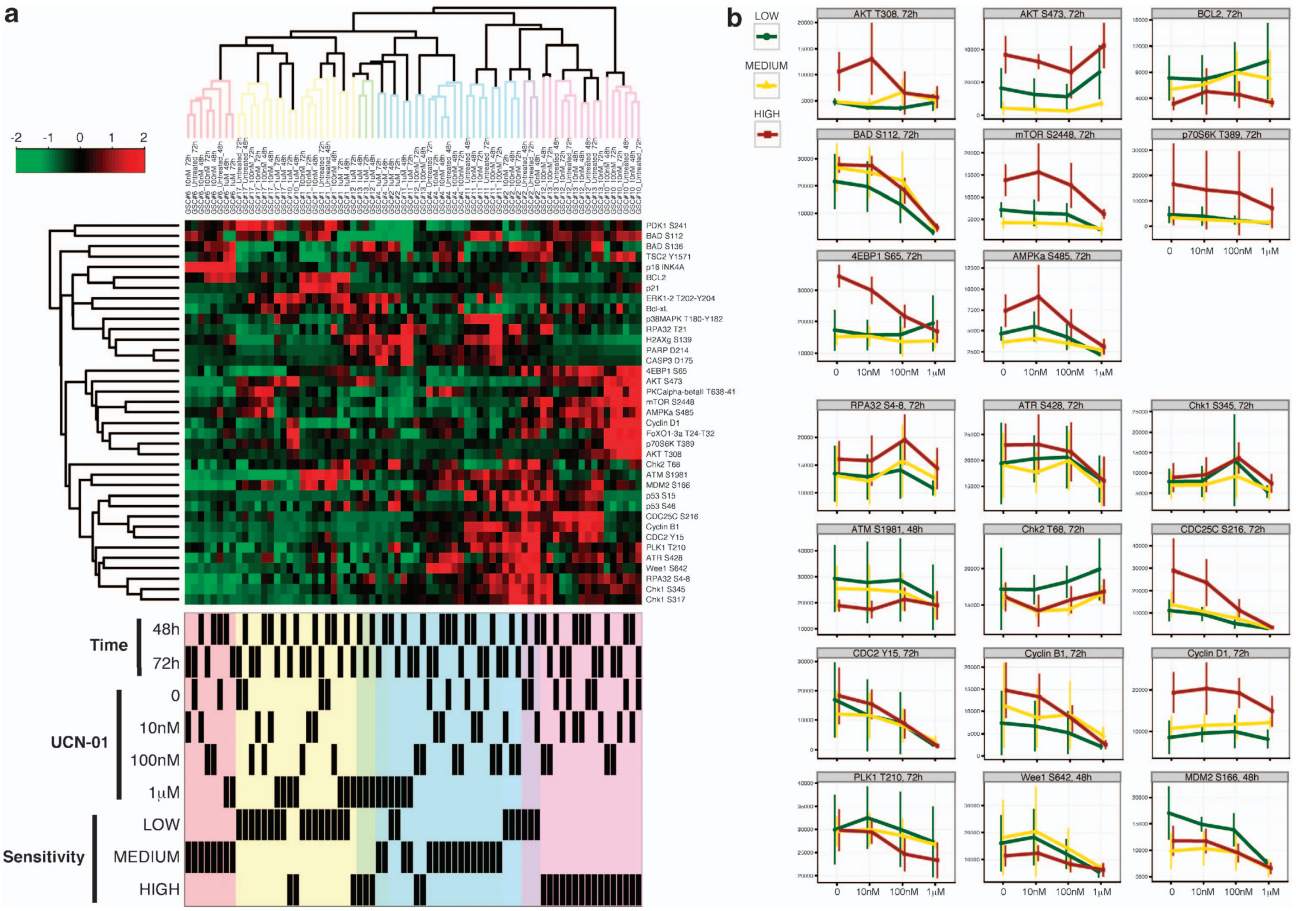

Figure 4 RPPM analysis on GSCs treated with UCN-01. (**a**) Annotated hierarchical clustering heatmaps of RPPM data obtained on nine GSCs treated with DMSO (untreated or 0) or increasing concentrations of UCN-01. Most analytes detected are part of the DNA damage response, cell cycle, and PI3K/AKT/mTOR pathways. Data for each GSCs represent the mean of three technical replicates. (**b**) Normalized intensity plots of end points extracted from the RPPM data and involved in the PI3K/AKT/mTOR, DNA-damage response, and cell cycle pathways. Mean and SD ($n=3$) for each sensitivity group are connected by solid, colored lines at increasing concentrations of UCN-01. The name of the analyte and the time point are reported on top of every single plot

respectively ($P<0.0001$, Figure 5c). In addition, treatment with UCN-01 dramatically lowered the density of tumor cells in the grafted striatum that scored 129.6 ± 8.89 and 15.13 ± 3.62 (mean ± S.E.M.) cells per high-power field in control and UCN-01-treated mice, respectively ($P<0.0001$, Figure 5d). Agglomerates of autofluorescent cell debris were observed at the brain site where UCN-01 was injected; pathological changes of the brain parenchyma, like poroencephalic cysts or glial scarring suggestive of potential UCN-01 toxicity, were not found.

Repeated injections of UCN-01 significantly reduce the growth of established GSC subcutaneous xenografts. In order to evaluate the effects of repeated injections of UCN-01 on established tumor xenografts, we subcutaneously implanted GSC 1 cells in the right flank of nude athymic mice. When tumors reached an average diameter of 10–13 mm, animals were treated with an intraperitoneal (i.p.) injection of UCN-01 (5 mg/kg in 0.15 ml of saline/15% DMSO, $n=5$) or vehicle alone (0.15 ml, $n=5$) every other day for 3 weeks (3 days per week, total of 9 injections). Although it has been demonstrated that the unbound fraction of UCN-01 in human plasma is very low because of binding to α1-acid glycoprotein, protein binding has not been reported in mice.[36,37] After the end of the treatment cycle, mice remained under observation for additional 3 weeks (Figure 6a). UCN-01 was well tolerated and no signs of toxicity were noted during the duration of the study. The diameter of the tumors in vehicle-treated mice progressively increased in size from 11.5 ± 0.39 to 23.6 ± 1.08 mm (mean ± S.E.M.), whereas a marked reduction of tumor growth rate was observed after the first UCN-01 treatment cycle (Figure 6b). The effects of UCN-01 continued after the second cycle of treatment and tumors had significantly smaller diameters as compared with control animals (13 ± 0.55 mm *versus* 14.8 ± 0.37 mm, mean ± S.E.M., $P=0.027$). Upon cessation of UCN-01 treatment, tumors resumed growth at a rate similar to control animals. Control tumors displayed the typical histological pattern of GSC xenografts[22] (Figure 6c). Prominent features were extensive areas of necrosis, arrangement of tumor cells in perinecrotic palisades, and remarkable angiogenesis. The tumor cells were rounded or polygonal in shape, conferring to the tumor parenchyma an epithelioid appearance. In xenografts treated with UCN-01, the tumor parenchyma was crossed by fibrous septa that separated clusters of tumor cells with elongated

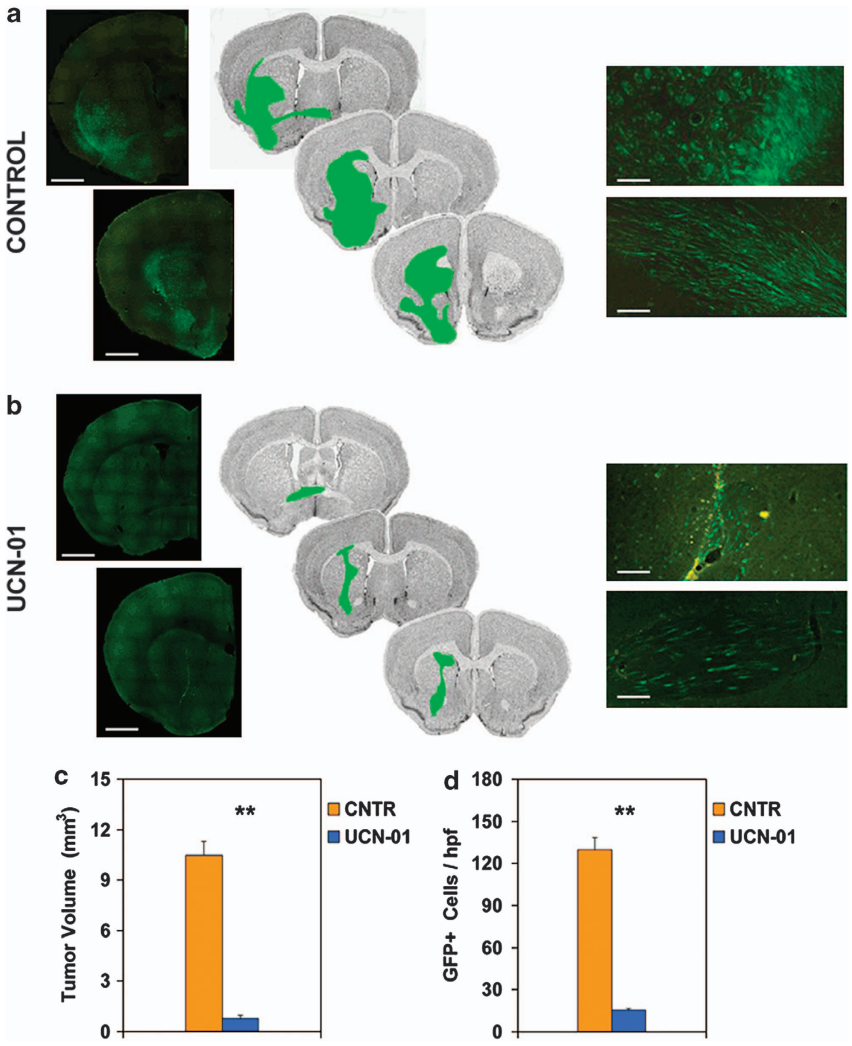

Figure 5 Effects of UCN-01 on the growth of intracerebral GFP-expressing GSC xenografts. (**a**) By 8 weeks after grafting, control mice showed tumor cells in the homolateral striatum, piriform cortex, corpus callosum, anterior commissure, internal capsule, optic tract, septal nuclei, and fimbria-hippocampus. (Left panel) Photomontage of two adjacent coronal brain sections 240 μm apart (scale bars, 1100 μm); (middle panel) schematic drawings of three adjacent sections 120 μm apart showing area demarcation for calculating tumor volume; (right panel) density of tumor cells in the grafted striatum (upper picture) and anterior commissure (lower picture) (scale bars, 140 μm). (**b**) Brain specimen of UCN-01-treated mouse showing inhibited growth and infiltrative potential by GSCs (left panel, scale bars, 1100 μm; right panel, scale bars, 140 μm). The brain area injected with UCN-01 showed autofluorescent cell debris without remarkable changes of the brain parenchyma (upper right panel). (**c** and **d**) Diagrams showing that both the volume of the brain region invaded by the GFP-expressing GSCs and the density of these cells in the grafted striatum are significantly smaller in UCN-01-treated mice as compared with controls (**$P<0.0001$)

morphology (Figure 6c). Fibrous healing tissue was detected in several areas both at the center and at the periphery of xenografts, suggesting that regressive phenomena had occurred within the tumor. Mitotic index in this tumor was significantly lower than in control xenografts (1.47 ± 0.17 *versus* 3.09 ± 0.37, mean $\pm$ S.E.M., $P<0.002$). To compare the *in vivo* effect of UCN-01 systemic treatment between low-, medium-, and high-sensitive GSCs, we chose subcutaneous grafting of Matrigel implants in immunodeficient mice that provide a well-suited model to study the early stages of *in vivo* tumor growth.[38] Histological examination showed that at 4 weeks after grafting, the implants are populated by clusters of tumor cells that strongly express GFP on fluorescence microscopy (Supplementary Figure S8a). Quantitative image analysis of GFP-expressing cells revealed that UCN-01 significantly reduced tumor cell density in the implants (Supplementary Figure S8a). Density of fluorescent tumor cells was 19.43 ± 0.63 (mean $\pm$ S.E.M.) and 15.63 ± 0.69 in control and UCN-01-treated GSC line 1 xenografts, respectively ($P<0.02$, Student's *t*-test), 26.17 ± 1.74 and 19.60 ± 1.22 in control and UCN-01-treated GSC line 6 xenografts, respectively ($P<0.01$), and 30.19 ± 1.58 and 11.3 ± 1.14 in control and UCN-01-treated GSC line 12 xenografts, respectively ($P<0.001$) (Supplementary Figure S8a). Immunostaining with anti-Ki67 showed that cell proliferation was significantly lowered in UCN-01-treated xenografts as compared with paired controls (Supplementary Figure S8b). The proliferation index was $4.01 \pm 0.21\%$ (mean $\pm$ S.E.M.) and $2.21 \pm 0.45\%$ in control and UCN-01-treated GSC line 1 xenografts, respectively ($P<0.002$), $5.87 \pm 0.71\%$ and $1.93 \pm 0.36\%$ in control and UCN-01-treated GSC line 6 xenografts, respectively

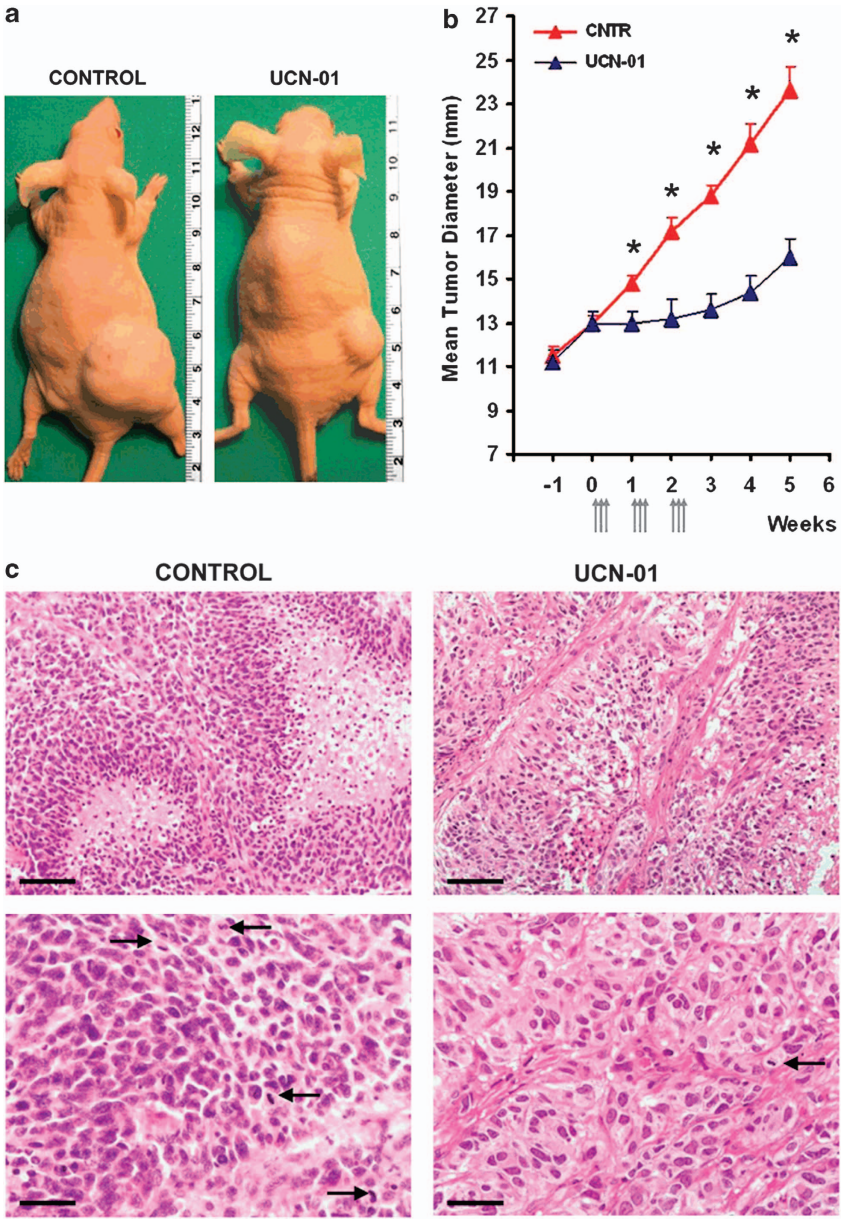

Figure 6 Effects of UCN-01 treatment on established subcutaneous xenografts. (**a**) Subcutaneous nodules in a control and UCN-01-treated mouse by 3 weeks after the end of treatment. (**b**) Growth curves of tumor xenografts in control and UCN-01-treated mice. The tumor size reached 1 week before starting UCN-01 administration (arrows) is indicated at the time point −1. The time point 0 corresponds to the beginning of treatment. Values are expressed as means ± S.E.M. *$P<0.01$. (**c**) Histological pattern of control and UCN-01-treated tumors. Control tumors showed the typical GBM pattern with foci of necrosis, perinecrotic pseudopalisades, angiogenic phenomena, and frequent mitotic figures (arrows). In UCN-01-treated tumors, clusters of tumor cells with elongated morphology were separated by septa of fibrous tissue. The density of tumor cells and mitosis was much lower than in control tumors. Mitotic index was significantly lower in UCN-01-treated tumors than in controls (1.47 ± 0.17 *versus* 3.09 ± 0.37, mean ± S.E.M., $P<0.002$). Scale bars, 140 μm (upper panels), 50 μm lower panels)

($P<0.001$), and 4.73 ± 1.06% and 1.07 ± 0.28% in control and UCN-01-treated GSC line 12 xenografts, respectively ($P<0.0001$) (Supplementary Figure S8b). Overall, these data confirmed that *in vivo* treatment fully reproduced the differential response to UCN-01 observed *in vitro*.

Discussion

The use of concurrent and sequential TMZ is the standard adjuvant treatment for GBM.[39] In the present study, we used patient-derived GSC lines and showed that prolonged treatment with TMZ does not significantly impair GSC survival that correlates with the absence of changes in many key signaling proteins involved in GSC proliferation and survival. TMZ is an alkylating agent and its efficacy is dependent on *MGMT* promoter methylation;[40] treatment with TMZ is not curative for GBM, possibly because of the concomitant activation of pathways other than DNA repair. In fact, inhibitors of MEK1/2 or SRC signaling are known to enhance CHK1 inhibitor lethality in primary human GBM cell lines, and although the mechanism seems to be mediated by caspases, overexpression of

Bcl-X_L alleviates but does not completely abolish MEK1/2 and CHK1 inhibitor cytotoxicity in GBM cells.[41] These findings suggest that concomitant inhibition of multiple proliferation/pro-survival and DNA damage/checkpoint pathways is necessary to efficiently kill glioma cells. Indeed, GSCs display elevated activity in multiple receptor tyrosine kinases, and the combination of sunitinib and gefitinb as well as sunitinib and sorafenib is effective *in vitro*.[17]

The protein signaling end points analyzed in our work are components of the EGF-R, AKT, mTOR, MAPK, TGF-β, WNT, and IGF-R pathways, most of which are known to be deregulated in GBM.[2] We found that preexisting activation of a variety of signaling proteins could be related to resistance of GSCs to TMZ treatment. Therefore, we tested the effects of a library of 80 small molecule inhibitors on GSCs. Five compounds passed the initial high-concentration screening and all of them failed in maintaining their efficacy at nanomolar concentrations. Treatment with analog compounds showed that, differently from all other molecules tested in this study, UCN-01 stratifies GSCs into three main classes of sensitivity.

UCN-01 is a staurosporine derivative that is far less promiscuous than its parent molecule, with significant activity against a handful of kinases. In particular, UCN-01 targets PDK1, PKC, and CHK1 (UCN-01/Staurosporine Kinome Interaction heatmaps are available at SuperNova Life Science, http://www.supernovalifescience.com). Pollack *et al.*[42–45] demonstrated significant activity of UCN-01 both *in vitro* on glioma cell lines and *in vivo* on U87MG xenografts. The concentrations of UCN-01 used *in vitro* in the cited studies range from 20 to 200 nM that caused significant effects only on 6 out of 20 GSC lines tested in the present work. The elevated concentration of UCN-01 needed to kill most GSCs suggests that simultaneous inhibition of multiple kinases may be required. Interestingly, UCN-01 efficacy does not correlate with PKC inhibition. These data are in line with experiments performed by others using Ro 31–8220, a staurosporine analog that targets a panel of kinases comparable to UCN-01, but with different potency.[46] Similarly, although many positive hits from our library screening are known to target PKC, here we show that two selective PKC inhibitors, Go 6976 and Ro 32-0432, do not efficiently kill GSCs at submicromolar concentrations, confirming that inhibition of PKC alone does not induce cell death in GSCs. This hypothesis is supported by the results of the combination assays of Ro 32-0432 with AZD7762 or OSU-03012, specific inhibitors of CHK1 and PDK1, respectively. In these experiments, addition of Ro 32-0432 does not result in a significant increase in the cell death induced by either AZD7762 or OSU-03012, whereas the combined effects of PDK1 and CHK1 inhibition reproduce those of UCN-01.

Our western blot data show that in most GSC lines tested, UCN-01 treatment causes a decrease of CDC25C, CDC2, and, at a lower extent, PKC phosphorylation but not of PDK1 phosphorylation. However, RPPM analysis of signaling downstream of PDK1 revealed that pAKT T308, which is the direct phosphorylation target of PDK1, is specifically affected by UCN-01 treatment in highly sensitive GSCs, confirming that PDK1 auto-phosphorylation (S241) may not be a reliable marker of the kinase activity.[47] The involvement of PDK1 in determining the different UCN-01 sensitivity of GSCs was also suggested by a significantly higher pPDK1 S241/PDK1 ratio in highly sensitive GSC lines compared with the other two groups. A model has been proposed for activation of PKC by PDK1,[48] and unlike its interaction with PKB/AKT, PDK1 has been shown to activate PKC independently of PTEN and 3′-phosphoinositides.[49] Recently, it has been demonstrated that PDK1 can activate PKC-ι, an atypical PKC isoform with oncogenic properties,[30] and as UCN-01 binds selectively to PDK1,[29] its efficacy may be partially explained by down-modulation of this signaling axis. The absence of activity on GSCs displayed by all selective PKC inhibitors used in our study and the lack of a dose-dependent decrease of PKC phosphorylation after UCN-01 treatment might also be explained by their selectivity against PKC-α and -β isoforms. RPPM analysis of the PI3K/AKT/mTOR signaling pathway revealed that GSCs with the highest sensitivity to UCN-01 display significantly elevated basal levels of pAKT S473 and, accordingly, of all phosphoproteins interacting within the mTOR pathway. Consistently, the presence of elevated inhibitory AMPKα phosphorylation (S485) suggests that sensitivity to UCN-01 is related to a preexisting activation of pro-survival and cell growth pathways, in line with the notion that mTOR signaling plays a critical role in cancer and, in particular, in GBM[50,51] (Supplementary Figure S7).

The observed decrease of CDC25C and CDC2 phosphorylation by western blot demonstrates that, besides acting on PDK1 and PKC, UCN-01 downregulates the activity of CHK1 and CDK1 in GSCs. It has been shown that radioresistance of GSCs can be reversed with specific inhibition of the CHK1 and CHK2 checkpoint kinases, thus confirming the relevance of DNA-damage pathways in GSC survival.[9] Our RPPM analysis of DNA-damage pathway in GSCs treated with UCN-01 confirms western blot data and shows the inhibitory phosphorylations of the CDC25C phosphatase and of CDC2 decrease in all GSCs in a dose-dependent manner. Moreover, compared with the other lines, the highly sensitive GSCs display higher basal levels of pRPA2 S4–8 and pATR S428, indicating that CHK1 signaling has an important role in mediating UCN-01 effects. Conversely, the presence of high levels of activatory MDM2 and ATM phosphorylations and of the inhibitory phosphorylation of WEE1 in the low/medium-sensitivity group, coupled to an increased activation of the ATM effector CHK2 only in the GSC group with the lowest sensitivity to UCN-01, suggests that these cells may experience less replicative stress if compared with highly sensitive GSCs (Supplementary Figure S7).

Collectively, our RPPM data underline the importance in GSCs of the molecular interplay between DNA damage and PI3K/AKT/mTOR signaling cascades. These pathways, which have been recently shown to be deranged in most cancers and, in particular, in GBM,[50,52,53] control cellular responses to genotoxic stress and are targeted by UCN-01.

The antitumor effect of UCN-01 is confirmed *in vivo* in either orthotopic or heterotopic models. In the latter, tumor growth inhibition is maintained after three cycles of administration, and even though after its cessation tumors started to grow at a rate similar to untreated controls, histologic examination revealed regressive phenomena within the tumor coupled to a significantly lower mitotic index than in control xenografts.

Taken together, our results show that UCN-01 efficiently kills GSCs *in vitro* and *in vivo*, and as the concomitant activation of multiple kinases remains a major issue in therapeutic intervention against GBM,[18–20] we suggest a rationale for simultaneous targeting of the PDK1 and CHK1 pathways. Finally, we confirm the utility of GSCs as a surrogate of the molecular heterogeneity of GBM and as a proxy for individualized drug screening.

Materials and Methods

Cell culture and drugs. GSCs were obtained from primary tumors as previously described.[3,23] The *O*6-methylguanine-DNA methyl transferase (*MGMT*) promoter methylation patterns were analyzed as previously described.[23] Normal adult neural stem cells (NS5) were obtained as previously described.[27]

GBM cell lines U87MG and T98G were purchased from ATCC (Manassas, VA, USA) and were cultivated in the recommended media (see www.atcc.org for details). TMZ and UCN-01 were purchased from Sigma (Sigma Aldrich Inc., Saint Louis, MO, USA), the small molecule kinase inhibitor library was from Enzo Life Sciences/Biomol (Farmingdale, NY, USA http://www.enzolifesciences.com/BML-2832/kinase-inhibitor-library), gefitinib, sorafenib, AZD7762 and OSU-03012 were from Selleck Chemicals (Houston, TX, USA) whereas PKC and ERK inhibitors were from Merck (Merck KGaA, Darmstadt, Germany) and Ro 32-0432 was from Tocris Bioscience (Bristol, UK).

Reverse-phase protein microarrays. RPPMs were performed as previously described.[54] Briefly, cell lysates were diluted with 2 × Tris-Glycine SDS Sample Buffer (Life Technologies Corporation, Carlsbad, CA, USA) before printing on nitrocellulose slides (Grace Bio-Labs, Bend, OR, USA) and were spotted in triplicate with the Aushon 2470 contact pin arrayer (AushonBioSystems Inc., Billerica, MA, USA), in 4-point twofold dilution curves. All antibodies used in these experiments are listed in Supplementary Table S5.

Western blot. Cell pellets were lysed in RIPA buffer: 150 mM NaCl, 10 mM Tris-HCl, 1 mM EDTA, and 1% Triton-X100 and Protease Inhibitor Cocktail (Sigma Aldrich). Samples were resolved on 4–12% SDS-PAGE gels and transferred to Hybond-C extra nitrocellulose (Amersham Pharmacia Biotech, Piscataway, NJ, USA). Antibodies used in these experiments are listed in Supplementary Table S5. Anti-β-actin antibody (Sigma Aldrich) was used as loading control. Quantification of the bands was performed by using ImageJ v1.47 (National Institutes of Health, Bethesda, MD, USA, http://imagej.nih.gov/ij/) and intensities of the bands for each antibody tested were normalized over their correspondent actin.

Cell cycle, TUNEL, and acridine orange/propidium iodide assays. Following mechanical dissociation, GSCs were plated in six-well microtiter plates for cell cycle analysis and terminal deoxynucleotidyl transferase dUTP nick-end labeling (TUNEL) assay. For acridine orange/propidium iodide (AO/PI) staining, cells were plated in 96-well microtiter plates (Ibidi, Martinsried, Germany). After 16 h, GSCs were treated with UCN-01 at a final concentration of 1 μM, and assays were performed either at 24 or 48 h thereafter.

Intracranial implantation of GSCs and histological assessment of tumor xenografts. Experiments involving animals were approved by the Ethical Committee of the Catholic University School of Medicine, Rome. NOD-SCID mice (Charles Rives, Milan, Italy) were implanted intracranially with 2×10^5 GFP-expressing GSCs in 5 μl of DMEM containing 1 μM UCN-01. Control mice were injected with equal number of GSCs in 5 μl of DMEM containing vehicle only. For grafting, the mice were anesthetized with i.p. injection of diazepam (20 mg/kg), followed by intramuscular injection of ketamine (40 mg/kg). After 8 weeks of survival, the mice were deeply anesthetized and transcardially perfused with 0.1 M PBS (pH 7.4), followed by 4% PFA in 0.1 M PBS. The brain was removed, stored in 30% sucrose buffer overnight at 4°C, frozen, and serially sliced at 20 μm on the coronal plane. Sections were collected in distilled water and mounted on slides with Vectashield mounting medium (Bio-Optica, Milan, Italy). Images were acquired with a laser scanning confocal microscope (LSM 500 META, Zeiss, Arese, Milan, Italy).

Subcutaneous grafting of GSCs, fluorescence microscopy, histology, and immunohistochmistry of tumor xenografts. Nude male athymic mice (Charles River) were implanted subcutaneously with 2×10^5 GSCs. For grafting, the cells were resuspended in 0.1 ml of cold PBS and the suspension mixed with an equal volume of cold Matrigel (Becton Dickinson, Franklin Lakes, NJ, USA). Tumor diameter was measured using a caliper and calculated as the mean value between the shortest and the longest diameters. Treatment with UCN-01 was initiated when the xenografts reached 10–13 mm in mean diameter, a size at which any change can be readily detected by caliper. UCN-01 (5 mg/kg in 0.15 ml of saline/15% DMSO) was injected i.p. once daily for 3 weeks (3 days per week; total 9 injections). UCN-01-treated mice ($n = 5$) were maintained up to 3 weeks without any further treatment, except for measurement of tumor mass, and then killed with an overdose of barbiturate. Controls mice ($n = 5$) received an equal volume of saline/15% DMSO that was injected i.p. For histologic examination of the tumors, mice were deeply anesthetized and transcardially perfused with 0.1 M PBS (pH 7.4), followed by 4% PFA in 0.1 M PBS. The implants were surgically removed and embedded in paraffin.

To compare the *in vivo* effect of UCN-01 between GSC lines belonging to low-, medium-, and high-sensitivity groups, 2×10^5 GFP-expressing cells of GCSs line 1, line 6, and line 12 were implanted subcutaneously. UCN-01 (5 mg/kg in 0.15 ml of saline/15% DMSO) was injected i.p. once daily for 3 weeks (3 days per week; total 9 injections). Controls included mice intraperitoneally injected with an equal volume of saline/15% DMSO. Matrigel implants were removed 4 weeks after grafting under magnified vision, stored in 30% sucrose buffer overnight at 4°C, and either cryotomed at 20 μm or embedded in paraffin and sectioned at 3 μm for evaluation of cell density and Ki67 immunostaining, respectively.

Statistical analysis. For RPPM data analysis, unsupervised hierarchical clustering (euclidean distance and Ward's method of linkage) was performed on standardized data using JMP v10.0.2 (SAS Institute, Cary, NC, USA) or 'R' software[55] (Bioconductor[56] and package 'Heatplus').

For *in vivo* data, differences in tumor volume, diameter, density of GSCs, and MI between the UCN-01-treated and control group were evaluated using Student's *t*-test. Statistical significance was assigned to *P*-values of < 0.05.

Conflict of Interest

The authors declare no conflict of interest.

Acknowledgements. This work was supported by grant from Associazione Italiana per la Ricerca sul Cancro (AIRC; start-up 6326 to LR-V) and by Fondi d'Ateneo, Linea D1, to RP.

1. Schwartzbaum JA, Fisher JL, Aldape KD, Wrensch M. Epidemiology and molecular pathology of glioma. *Nat Clin Pract Neurol* 2006; **2**: 494–503; quiz 491 p following 516.
2. Tanaka S, Louis DN, Curry WT, Batchelor TT, Dietrich J. Diagnostic and therapeutic avenues for glioblastoma: no longer a dead end? *Nat Rev Clin Oncol* 2013; **10**: 14–26.
3. Eramo A, Ricci-Vitiani L, Zeuner A, Pallini R, Lotti F, Sette G *et al.* Chemotherapy resistance of glioblastoma stem cells. *Cell Death Differ* 2006; **13**: 1238–1241.
4. Weller M, Stupp R, Hegi M, Wick W. Individualized targeted therapy for glioblastoma: fact or fiction? *Cancer J* 2012; **18**: 40–44.
5. Singh SK, Hawkins C, Clarke ID, Squire JA, Bayani J, Hide T *et al.* Identification of human brain tumour initiating cells. *Nature* 2004; **432**: 396–401.
6. Galli R, Binda E, Orfanelli U, Cipelletti B, Gritti A, De Vitis S *et al.* Isolation and characterization of tumorigenic, stem-like neural precursors from human glioblastoma. *Cancer Res* 2004; **64**: 7011–7021.
7. Nduom EK, Hadjipanayis CG, Van Meir EG. Glioblastoma cancer stem-like cells: implications for pathogenesis and treatment. *Cancer J* 2012; **18**: 100–106.
8. Teodorczyk M, Martin-Villalba A. Sensing invasion: cell surface receptors driving spreading of glioblastoma. *J Cell Physiol* 2010; **222**: 1–10.
9. Bao S, Wu Q, McLendon RE, Hao Y, Shi Q, Hjelmeland AB *et al.* Glioma stem cells promote radioresistance by preferential activation of the DNA damage response. *Nature* 2006; **444**: 756–760.
10. Ricci-Vitiani L, Pallini R, Biffoni M, Todaro M, Invernici G, Cenci T *et al.* Tumour vascularization via endothelial differentiation of glioblastoma stem-like cells. *Nature* 2010; **468**: 824–828.
11. Cheng L, Huang Z, Zhou W, Wu Q, Donnola S, Liu JK *et al.* Glioblastoma stem cells generate vascular pericytes to support vessel function and tumor growth. *Cell* 2013; **153**: 139–152.
12. Cancer Genome Atlas Research Network. Comprehensive genomic characterization defines human glioblastoma genes and core pathways. *Nature* 2008; **455**: 1061–1068.

13. Phillips HS, Kharbanda S, Chen R, Forrest WF, Soriano RH, Wu TD *et al.* Molecular subclasses of high-grade glioma predict prognosis, delineate a pattern of disease progression, and resemble stages in neurogenesis. *Cancer Cell* 2006; **9**: 157–173.
14. Verhaak RG, Hoadley KA, Purdom E, Wang V, Qi Y, Wilkerson MD *et al.* Integrated genomic analysis identifies clinically relevant subtypes of glioblastoma characterized by abnormalities in PDGFRA, IDH1, EGFR, and NF1. *Cancer Cell* 2010; **17**: 98–110.
15. Lassman AB, Abrey LE, Gilbert MR. Response of glioblastomas to EGFR kinase inhibitors. *N Engl J Med* 2006; **354**: 525–526; author reply 525-526.
16. Kozuka-Hata H, Tasaki S, Oyama M. Phosphoproteomics-based systems analysis of signal transduction networks. *Front Physiol* 2011; **2**: 113.
17. Joshi AD, Loilome W, Siu IM, Tyler B, Gallia GL, Riggins GJ. Evaluation of tyrosine kinase inhibitor combinations for glioblastoma therapy. *PLoS One* 2012; **7**: e44372.
18. Clark PA, Iida M, Treisman DM, Kalluri H, Ezhilan S, Zorniak M *et al.* Activation of multiple ERBB family receptors mediates glioblastoma cancer stem-like cell resistance to EGFR-targeted inhibition. *Neoplasia* 2012; **14**: 420–428.
19. Szerlip NJ, Pedraza A, Chakravarty D, Azim M, McGuire J, Fang Y *et al.* Intratumoral heterogeneity of receptor tyrosine kinases EGFR and PDGFRA amplification in glioblastoma defines subpopulations with distinct growth factor response. *Proc Natl Acad Sci USA* 2012; **109**: 3041–3046.
20. Jun HJ, Acquaviva J, Chi D, Lessard J, Zhu H, Woolfenden S *et al.* Acquired MET expression confers resistance to EGFR inhibition in a mouse model of glioblastoma multiforme. *Oncogene* 2012; **31**: 3039–3050.
21. Davis MI, Hunt JP, Herrgard S, Ciceri P, Wodicka LM, Pallares G *et al.* Comprehensive analysis of kinase inhibitor selectivity. *Nat Biotechnol* 2011; **29**: 1046–1051.
22. Ricci-Vitiani L, Pallini R, Larocca LM, Lombardi DG, Signore M, Pierconti F *et al.* Mesenchymal differentiation of glioblastoma stem cells. *Cell Death Differ* 2008; **15**: 1491–1498.
23. Pallini R, Ricci-Vitiani L, Banna GL, Signore M, Lombardi D, Todaro M *et al.* Cancer stem cell analysis and clinical outcome in patients with glioblastoma multiforme. *Clin Cancer Res* 2008; **14**: 8205–8212.
24. Hammond LA, Eckardt JR, Baker SD, Eckhardt SG, Dugan M, Forral K *et al.* Phase I and pharmacokinetic study of temozolomide on a daily-for-5-days schedule in patients with advanced solid malignancies. *J Clin Oncol* 1999; **17**: 2604–2613.
25. Paweletz CP, Charboneau L, Bichsel VE, Simone NL, Chen T, Gillespie JW *et al.* Reverse phase protein microarrays which capture disease progression show activation of pro-survival pathways at the cancer invasion front. *Oncogene* 2001; **20**: 1981–1989.
26. Wulfkuhle JD, Edmiston KH, Liotta LA, Petricoin 3rd EF. Technology insight: pharmacoproteomics for cancer–promises of patient-tailored medicine using protein microarrays. *Nat Clin Pract Oncol* 2006; **3**: 256–268.
27. Ricci-Vitiani L, Pedini F, Mollinari C, Condorelli G, Bonci D, Bez A *et al.* Absence of caspase 8 and high expression of PED protect primitive neural cells from cell death. *J Exp Med* 2004; **200**: 1257–1266.
28. Zhao B, Bower MJ, McDevitt PJ, Zhao H, Davis ST, Johanson KO *et al.* Structural basis for Chk1 inhibition by UCN-01. *J Biol Chem* 2002; **277**: 46609–46615.
29. Komander D, Kular GS, Bain J, Elliott M, Alessi DR, Van Aalten DM. Structural basis for UCN-01 (7-hydroxystaurosporine) specificity and PDK1 (3-phosphoinositide-dependent protein kinase-1) inhibition. *Biochem J* 2003; **375**(Pt 2): 255–262.
30. Davies SP, Reddy H, Caivano M, Cohen P. Specificity and mechanism of action of some commonly used protein kinase inhibitors. *Biochem J* 2000; **351**(Pt 1): 95–105.
31. Gani OA, Engh RA. Protein kinase inhibition of clinically important staurosporine analogues. *Nat Prod Rep* 2010; **27**: 489–498.
32. Akinaga S, Gomi K, Morimoto M, Tamaoki T, Okabe M. Antitumor activity of UCN-01, a selective inhibitor of protein kinase C, in murine and human tumor models. *Cancer Res* 1991; **51**: 4888–4892.
33. Fruman DA, Rommel C. PI3K and cancer: lessons, challenges and opportunities. *Nat Rev Drug Discov* 2014; **13**: 140–156.
34. Bhat KP, Balasubramaniyan V, Vaillant B, Ezhilarasan R, Hummelink K, Hollingsworth F *et al.* Mesenchymal differentiation mediated by NF-kappaB promotes radiation resistance in glioblastoma. *Cancer Cell* 2013; **24**: 331–346.
35. Lee J, Kotliarova S, Kotliarov Y, Li A, Su Q, Donin NM *et al.* Tumor stem cells derived from glioblastomas cultured in bFGF and EGF more closely mirror the phenotype and genotype of primary tumors than do serum-cultured cell lines. *Cancer Cell* 2006; **9**: 391–403.
36. Fuse E, Tanii H, Kurata N, Kobayashi H, Shimada Y, Tamura T *et al.* Unpredicted clinical pharmacology of UCN-01 caused by specific binding to human alpha1-acid glycoprotein. *Cancer Res* 1998; **58**: 3248–3253.
37. Fuse E, Kuwabara T, Sparreboom A, Sausville EA, Figg WD. Review of UCN-01 development: a lesson in the importance of clinical pharmacology. *J Clin Pharmacol* 2005; **45**: 394–403.
38. Falchetti ML, Mongiardi MP, Fiorenzo P, Petrucci G, Pierconti F, D'Agnano I *et al.* Inhibition of telomerase in the endothelial cells disrupts tumor angiogenesis in glioblastoma xenografts. *Int J Cancer* 2008; **122**: 1236–1242.
39. Stupp R, Mason WP, van den Bent MJ, Weller M, Fisher B, Taphoorn MJ *et al.* Radiotherapy plus concomitant and adjuvant temozolomide for glioblastoma. *N Engl J Med* 2005; **352**: 987–996.
40. Hegi ME, Diserens AC, Gorlia T, Hamou MF, de Tribolet N, Weller M *et al.* MGMT gene silencing and benefit from temozolomide in glioblastoma. *N Engl J Med* 2005; **352**: 997–1003.
41. Tang Y, Dai Y, Grant S, Dent P. Enhancing CHK1 inhibitor lethality in glioblastoma. *Cancer Biol Ther* 2012; **13**: 379–388.
42. Bredel M, Pollack IF, Freund JM, Rusnak J, Lazo JS. Protein kinase C inhibition by UCN-01 induces apoptosis in human glioma cells in a time-dependent fashion. *J Neurooncol* 1999; **41**: 9–20.
43. Jane EP, Premkumar DR, Pollack IF. AG490 influences UCN-01-induced cytotoxicity in glioma cells in a p53-dependent fashion, correlating with effects on BAX cleavage and BAD phosphorylation. *Cancer Lett* 2007; **257**: 36–46.
44. Pollack IF, Kawecki S, Lazo JS. Blocking of glioma proliferation in vitro and in vivo and potentiating the effects of BCNU and cisplatin: UCN-01, a selective protein kinase C inhibitor. *J Neurosurg* 1996; **84**: 1024–1032.
45. Witham TF, Erff ML, Okada H, Chambers WH, Pollack IF. 7-Hydroxystaurosporine-induced apoptosis in 9L glioma cells provides an effective antigen source for dendritic cells and yields a potent vaccine strategy in an intracranial glioma model. *Neurosurgery* 2002; **50**: 1327–1334; discussion 1334-1325.
46. Han Z, Pantazis P, Lange TS, Wyche JH, Hendrickson EA. The staurosporine analog, Ro-31-8220, induces apoptosis independently of its ability to inhibit protein kinase C. *Cell Death Differ* 2000; **7**: 521–530.
47. Medina JR. Selective 3-phosphoinositide-dependent kinase 1 (PDK1) inhibitors: dissecting the function and pharmacology of PDK1. *J Med Chem* 2013; **56**: 2726–2737.
48. Collins BJ, Deak M, Murray-Tait V, Storey KG, Alessi DR. In vivo role of the phosphate groove of PDK1 defined by knockin mutation. *J Cell Sci* 2005; **118**(Pt 21): 5023–5034.
49. Freeley M, Park J, Yang KJ, Wange RL, Volkov Y, Kelleher D *et al.* Loss of PTEN expression does not contribute to PDK-1 activity and PKC activation-loop phosphorylation in Jurkat leukaemic T cells. *Cell Signal* 2007; **19**: 2444–2457.
50. Kahn J, Hayman TJ, Jamal M, Rath BH, Kramp T, Camphausen K *et al.* The mTORC1/mTORC2 inhibitor AZD2014 enhances the radiosensitivity of glioblastoma stem-like cells. *Neuro Oncol* 2014; **16**: 29–37.
51. Liu P, Cheng H, Roberts TM, Zhao JJ. Targeting the phosphoinositide 3-kinase pathway in cancer. *Nat Rev Drug Discov* 2009; **8**: 627–644.
52. Cam M, Bid HK, Xiao L, Zambetti GP, Houghton PJ, Cam H. p53/TAp63 and AKT regulate mammalian target of rapamycin complex 1 (mTORC1) signaling through two independent parallel pathways in the presence of DNA damage. *J Biol Chem* 2014; **289**: 4083–4094.
53. Budanov AV, Karin M. p53 target genes sestrin1 and sestrin2 connect genotoxic stress and mTOR signaling. *Cell* 2008; **134**: 451–460.
54. Pierobon M, Vanmeter AJ, Moroni N, Galdi F, Petricoin 3rd EF. Reverse-phase protein microarrays. *Methods Mol Biol* 2012; **823**: 215–235.
55. R Core Team. *R: A Language and Environment for Statistical Computing*. R Foundation for Statistical Computing: Vienna, Austria, 2013. http://www.R-project.org/.
56. Gentleman RC, Carey VJ, Bates DM, Bolstad B, Dettling M, Dudoit S *et al.* Bioconductor: open software development for computational biology and bioinformatics. *Genome Biol* 2004; **5**: R80.

Supplementary Information accompanies this paper on Cell Death and Disease website (http://www.nature.com/cddis)